Deterministic coupling of a single atom to a nanoscale optical cavity

Deterministic coupling of a single atom to a nanoscale optical cavity [v5.9]

J.D. Thompson,[1*] T.G. Tiecke,[1,2*], N.P. de Leon [1,3], J. Feist [1,4],
A.V. Akimov [1,5], M. Gullans [1], A.S. Zibrov [1], V. Vuletić, [2] M.D. Lukin[1†]

[1]Department of Physics, Harvard University, Cambridge MA 02138
[2]Department of Physics, MIT-Harvard Center for Ultracold Atoms,
and Research Laboratory of Electronics,
Massachusetts Institute of Technology, Cambridge, Massachusetts 02139
[3]Department of Chemistry and Chemical Biology, Harvard University, Cambridge MA 02138
[4]Wherever Johannes is now
[5]Russian Quantum Center, Skolkovo, Moscow Region, Russia.
[*]These authors contributed equally to this work.
[†]To whom correspondence should be addressed. Email: lukin@physics.harvard.edu

Deterministic control over interactions between isolated ultra-cold atoms and nanoscale solid-state systems is an outstanding problem in quantum science. It is of interest for understanding the fundamental limits of quantum control over complex systems, as well as for realizing hybrid quantum systems, combining the excellent coherence properties of atoms with strong interactions and scalability. We propose and demonstrate a technique for deterministically interfacing a single rubidium atom with a nanoscale photonic crystal cavity by trapping the atom in the near-field of the cavity. By controlling the atom's position, we probe the cavity field non-invasively with a resolution below the diffraction limit. The single-photon-single-atom coupling rate is $2\pi \times 580 \pm 80$

MHz, as measured by a reduction in the cavity transmission. Prospects for integrated, strongly-coupled quantum nano-optical circuits, and their potential applications, are discussed.

Trapped, ultra-cold atoms coupled to nanoscale optical cavities are exemplary hybrid quantum systems ([1–3]). The exceptional coherence lifetime of select atomic states and the strong atom-photon interactions arising from sub-wavelength photon localization represent a promising combination for potential applications ranging from single-photon nonlinear optics ([4–7]) to quantum networks ([8, 9]). However, in order to take advantage of the strong coupling in an efficient and scalable way, it is essential to gain control over individual trapped atoms very close to surfaces, within the near field of the confined optical mode. Specifically, the critical length scale is the reduced atomic resonance wavelength: $\lambda/2\pi \sim 125$ nm for rubidium. Lateral position control at this level has been achieved for single atoms in free space and in micrometer scale cavities using standing waves ([10–12]), or high numerical-aperture optics ([13–15]). Achieving similar control close the surface is much more challenging, because attractive atom-surface forces can exceed typical trapping forces for cold atoms in this regime. Previously, atomic ensembles have been stably trapped at distances down to 500 nm using magnetic traps formed by patterned electrodes ([16, 17]), and down to 230 nm using optical dipole traps based on evanescent waves ([18, 19]).

Our approach provides a high degree of control over the three-dimensional position of an atom near a nanoscale object, by using a tightly focussed optical tweezer beam ([20]) which is retro-reflected from the nanoscale object itself ([21–23]) (Figure 1a). The resulting standing-wave optical lattice has a local intensity maximum at a distance $z_0 \sim \lambda/4$ from the surface, and additional maxima farther away spaced in increments of $\lambda/2$. For an optical tweezer beam that is red-detuned from the atomic resonance, these intensity maxima correspond to potential energy minima, which can confine an atom along all axes. The lateral position of the trap can

2

be controlled by moving the focus of the optical tweezer, while the distance z_0 depends on the phase shift of the reflected light, which is determined by the geometry of the nanostructure. In certain cases, changing the structure dimensions allows z_0 to be tuned between nearly 0 and $\lambda/2$ (see Figs. S2, S3). Crucially, the closest lattice site at z_0 can be deterministically loaded with a single atom from a conventional free-space optical tweezer simply by scanning it onto and over the surface. Even though surface forces and realistic laser intensities limit the usable distance to about 100 nm (*24*), this method nevertheless allows for direct near-field coupling of atoms to solid-state nanostructures of interest.

Our experimental apparatus (Figs. 1a,b, S1), is built around a nanostructure, mounted to a tapered optical fiber tip. It is placed in the focal plane of a high numerical aperture lens inside an ultra-high vacuum chamber. A magneto-optical trap (MOT) is formed around the fiber tip, and used to load the optical tweezer ($1/e^2$ waist $w = 900$ nm, depth $U_0/k_B = 1.6$ mK) at a distance of $40\,\mu$m from the nanostructure. The presence of only a single atom is ensured by the collisional blockade effect (*25*). After a period of Raman sideband cooling (*26,27*), we load the atom into the lattice by translating the optical tweezer using a scanning galvanometer mirror (Fig. 1c) until it is aimed directly at the nanostructure.

We first validate our technique by positioning an atom near a bare tapered nanofiber tip (see figure 2a,b), without an additional nanostructure present. To determine the fraction of atoms loaded into the first lattice site, we measure the site populations spectroscopically. A weak, off-resonant probe beam guided by the nanofiber produces a state-dependent AC Stark shift for the ground state hyperfine levels, which is a strong function of the distance to the fiber surface (*24*). Figure 2c shows the microwave-frequency spectra obtained by focusing the tweezer in different z-planes before loading the lattice. Two distinct peaks appear: one near the unperturbed transition frequency at f_B, and another shifted by 150 kHz at f_A, which we identify as the resonance position in the lattice site closest to the fiber. This identification is

3

independently confirmed by measuring the fraction of the atomic fluorescence coupled into the fiber (*24*). Accounting only for well calibrated losses (detector quantum efficiency and a free space fiber coupling stage) we expect a collection efficiency in the closest (second closest) lattice site of 0.04 (0.002). The measured efficiency associated with peak f_A is $0.015(6)$, thereby confirming the loading of the closest trap. We conclude from the data in Fig. 2c that an atom in the free-space tweezer is loaded into the lattice with probability $0.94(6)$ (after correcting for independently measured losses from background gas collisions). Conditioned on successful loading into the lattice, the atom is in the first lattice site with probability $1.00^{+0.0}_{-0.12}$.

We next demonstrate coupling an atom to a photonic crystal waveguide cavity (PWC) (*28*). These devices can support high quality factor optical resonances and extremely small mode volumes, less than λ^3. Our PWC (Fig. 3a-c) is fabricated in silicon nitride. It is attached to a tapered optical fiber tip, which provides an efficient optical interface to the cavity in addition to mechanical support. Due to the nanoscale dimensions of the waveguide, a significant fraction of the electromagnetic field energy is contained in the evanescent region just outside the waveguide, which allows for significant coupling to an atom trapped in this region, without entering the holes in the waveguide as proposed previously (*29–31*). As shown in Fig. 1c, coupling strengths $g(r) = \mathbf{d} \cdot \mathbf{E}(\mathbf{r})/\hbar$ as high as several GHz are achievable in the range of distances accessible with the present technique.

To directly demonstrate that the atom couples to the localized cavity mode, we position an atom at various points along the waveguide axis to produce a map of the cavity intensity distribution. The local intensity is measured by pumping the cavity weakly with a laser tuned near the D2 line $F = 2 \rightarrow F' = 2$ transition, and measuring the time required to optically pump an atom from $|F = 2, m_F = -2\rangle$ to a dark state in $F = 1$. The result is shown in Fig. 3d, along with a simulation of the expected intensity distribution. The expected cavity mode is a standing wave (with a period given by the PWC lattice constant, $a \sim 290$ nm), modulated over

several microns by a gaussian-like envelope with two lobes. Both features are clearly visible in the data. To achieve good agreement in the contrast of the standing wave, the simulation is convolved with a gaussian point-spread function with a root-mean-square (rms) width of 95 nm. This blur arises from drift in the tweezer alignment over the course of the measurement (32 hours), position jitter in the galvanometer mirror and the thermal motion of the atom. Viewed as a non-invasive probe of the intra-cavity field distribution, this technique has a spatial resolution of $190(30)$ nm (Sparrow criterion (*32*)).

Next, we determine the atom-cavity coupling strength quantitatively by measuring the modification of the cavity transmission induced by the presence of an atom. Given the cooperativity $\eta \equiv (2g)^2/(\kappa\Gamma)$, where κ and Γ are the full linewidths of the cavity and the atomic excited $5P_{3/2}$ state, respectively, the transmission in the presence of an (unsaturated) resonant atom is given by $T = (1+\eta)^{-2}$ (*6,33*). To measure the transmission, we couple a weak probe field into the waveguide by scattering a focused beam off of the free-standing tip of the waveguide, and collect the transmitted light through the tapered optical fiber supporting the waveguide.

With the atom loaded at the position of the cavity mode maximum ($x = +0.8\,\mu$m in Fig. 3d), we record the transmission of light near the $F = 2 \rightarrow F' = 3$ transition as shown in Fig. 4. The atom decreases the cavity transmission by at most 2.2%, and the full-width at half-maximum (FWHM) of the transmission dip is about 26 MHz, or 4 times the natural linewidth. The decrease in the transmission persists for about 1 ms, during which time the atom scatters 60 photons. The lifetime of the atom in the absence of the probe field is 250 ms; the reduced lifetime with the probe is due to heating from photon scattering, which is likely dominated by fluctuating dipole forces associated with inhomogeneous trapping potentials for different magnetic sublevels in the ground state.

To understand the measured spectrum, we note that the linearly polarized cavity field does not drive a single, closed transition. Since each trapped atom scatters many cavity photons,

an atom starting in the $|2, -2\rangle$ magnetic sublevel is optically pumped to other sublevels in the $F = 2$ manifold during the measurement interval. The transitions originating from different magnetic sublevels have different frequencies due to a finite magnetic field and vector and tensor light shifts; therefore, for a given detuning only a fraction of the ground state population is resonant with the probe laser. This gives rise to a broadened spectrum that is slightly asymmetric (see also Fig. S6), with less reduction in the transmission than expected for a two-level atom. These effects could be eliminated by using a "magic wavelength" trap (*34*), or by using strong magnetic field to spectrally resolve the cycling $|2, 2\rangle \rightarrow |3, 3\rangle$ transition.

We have modeled these effects quantitatively using numerical simulations of the master equation for a Rb atom including the 12 relevant Zeeman states of the $F = 2 \rightarrow F' = 3$ transition (*24*), and find good agreement between the model, the data, and the predicted coupling strength. The model, shown by the red line in Fig. 4, yields an estimate of $\eta = 0.067(10)$ and cavity QED parameters of $(2g, \kappa, \Gamma) = 2\pi \times (0.58(8), 840(80), 0.006)$ GHz for the $|2, 0\rangle \rightarrow |3, 0\rangle$ transition. This is a conservative estimate, as we have not subtracted a background transmission channel arising from a higher-order waveguide mode that does not couple strongly to the atom. This result is in reasonable agreement with estimates based on numerical modeling of the optical potential and cavity geometry. Given the dimensions of this PWC and its orientation with respect to the optical tweezer propagation axis (Fig. S5), we expect the nanotrap to lie at a distance of $z_0 = 260$ nm from the surface, with $2g/(2\pi) \sim 800$ MHz on the $|2, 0\rangle \rightarrow |3, 0\rangle$ transition.

Several straightforward improvements can be made to improve the coupling strength. First, an optimized waveguide geometry will allow z_0 to be reduced to less than 130 nm, increasing $2g/(2\pi)$ to 3 GHz (*24*). Additionally, quality factors as high as $Q = 3 \times 10^5$ have already been demonstrated for SiN PWCs (*35*). These two improvements together give a cooperativity of $\eta > 1000$ and achieve the strong coupling regime of cavity QED $2g > (\kappa, \Gamma)$. Even stronger

6

coupling can potentially be accessed by trapping atoms inside holes in the waveguide, using alternate PWC geometries to create the necessary trapping potentials (*31, 36*).

The present technique opens up exciting prospects for realizing a wide variety of hybrid quantum systems. For example, the method can be used to deterministically load multiple traps on the same or different PWCs, or cavities forming a network in two dimensions on a chip. In combination with the parallel fabrication and integration possible with nano-photonics, this is a promising route towards realizing complex nano-optical circuits with many atomic qubits. Potential applications range from quantum nonlinear optics (*37*) to quantum networks (*8*) and novel many-body systems (*38*).

Beyond realizations of these novel quantum optical systems, our technique can be applied to implement quantum interfaces between ultra-cold atoms and mechanical oscillators (*39*), and explore direct coupling of atoms to electromagnetic circuits on a chip (*40*). Novel applications to nanoscale sensing and probing atom-surface interactions at sub-micron length scales can also be foreseen. Finally, the present technique may allow for new approaches to quantum control of single atoms at sub-wavelength length scales. Specifically, by starting from quantum-degenerate gas it might be possible to simultaneously load multiple near-field traps separated by distances considerably smaller than $\lambda/2$ (*41*). This may allow studies of strongly correlated states to be extended into a new regime of high atomic densities and strong, long-ranged interactions. In particular, new types of strongly correlated, coherent quantum matter can be created in the regimes in between dilute ultra-cold quantum gases and practical solid-state systems.

References and Notes

1. C. Monroe, M. Lukin, *Phys. World* **21**, 32 (2008).

2. M. Wallquist, K. Hammerer, P. Rabl, M. Lukin, P. Zoller, *Physica Scripta* **2009**, 014001

(2009).

3. P. Treutlein, C. Genes, K. Hammerer, M. Poggio, P. Rabl, *to appear in: "Cavity Optome-chanics", ed. by M. Aspelmeyer, T. Kippenberg, F. Marquardt (Springer), arXiv:1210.4151* (2012).

4. K. Birnbaum, *et al.*, *Nature* **436**, 87 (2005).

5. M. Hijlkema, *et al.*, *Nature* **3**, 253 (2007).

6. D. E. Chang, A. S. Sorensen, E. A. Demler, M. Lukin, *Nature Physics* **3**, 807 (2007).

7. I. Fushman, *et al.*, *Science* **320**, 769 (2008).

8. H. J. Kimble, *Nature* **453**, 1023 (2008).

9. C. Nölleke, *et al.*, *arXiv:1212.3127* (2012).

10. I. Dotsenko, *et al.*, *Phys. Rev. Lett.* **95**, 033002 (2005).

11. A. Reiserer, C. Nölleke, S. Ritter, G. Rempe, *arXiv:1212.5295* (2012).

12. R. Gehr, *et al.*, *Phys. Rev. Lett.* **104**, 203602 (2010).

13. J. Beugnon, *et al.*, *Nature Physics* **3**, 696 (2007).

14. W. S. Bakr, J. I. Gillen, A. Peng, S. Fölling, M. Greiner, *Nature* **462**, 74 (2009).

15. A. Lengwenus, J. Kruse, M. Schlosser, S. Tichelmann, G. Birkl, *Physical Review Letters* **105**, 170502 (2010).

16. Y. Lin, I. Teper, C. Chin, V. Vuletić, *Physical Review Letters* **92**, 50404 (2004).

17. D. Hunger, *et al.*, *Physical Review Letters* **104**, 143002 (2010).

18. E. Vetsch, *et al.*, *Physical Review Letters* **104**, 203603 (2010).

19. A. Goban, *et al.*, *Physical Review Letters* **109**, 033603 (2012).

20. N. Schlosser, G. Reymond, I. Protsenko, P. Grangier, *Nature* **411**, 1024 (2001).

21. R. A. Cornelussen, A. H. Van Amerongen, B. T. Wolschrijn, R. Spreeuw, H. B. van Linden van den Heuvell, *European Physical Journal D* **21**, 347 (2002).

22. J. Gillen, *et al.*, *Physical Review A* **80**, 021602 (2009).

23. M. Miranda, *et al.*, *Physical Review A* **86**, 063615 (2012).

24. Materials and methods are available as supplementary material on Science Online.

25. N. Schlosser, G. Reymond, P. Grangier, *Physical Review Letters* **89**, 023005 (2002).

26. J. D. Thompson, T. G. Tiecke, A. S. Zibrov, V. Vuletić, M. D. Lukin, *arxiv:1209.3028* (2012).

27. A. M. Kaufman, B. J. Lester, C. A. Regal, *Physical Review X* **2**, 041014 (2012).

28. P. R. Villeneuve, *et al.*, *Nature* **390**, 143 (1997).

29. J. Vuckovic, M. Loncar, H. Mabuchi, A. Scherer, *Physical Review E* **65**, 016608 (2002).

30. B. Lev, K. Srinivasan, P. Barclay, O. Painter, H. Mabuchi, *Nanotechnology* **15**, S556 (2004).

31. C. L. Hung, S. M. Meenehan, D. E. Chang, O. Painter, H. J. Kimble, *arXiv:1301.5252* (2013).

32. E. Hecht, *Optics* (Addison Wesley Longman, Reading, MA, 1998), third edn.

33. J. T. Shen, S. Fan, *Optics Letters* **30**, 2001 (2005).

34. J. Ye, H. J. Kimble, H. Katori, *Science* **320**, 1734 (2008).

35. M. Eichenfield, R. Camacho, J. Chan, K. J. Vahala, O. Painter, *Nature* **459**, 550 (2009).

36. D. van Oosten, L. Kuipers, *Phys. Rev. A* **84**, 011802 (2011).

37. T. Peyronel, *et al.*, *Nature* **488**, 57 (2012).

38. D. E. Chang, *et al.*, *Nature Physics* **4**, 884 (2008).

39. D. Hunger, *et al.*, *C. R. Physique* p. 871 (2011).

40. A. André, *et al.*, *Nature Physics* **2**, 636 (2006).

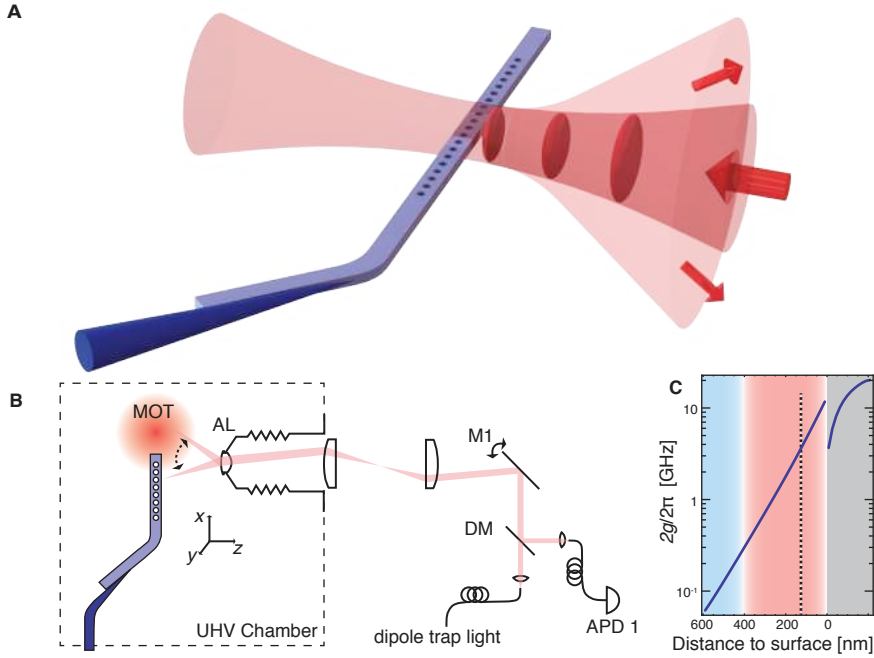41. M. Gullans, *et al.*, *Physical Review Letters* **109**, 235309 (2012).

Figure 1: Experimental concept. (a) The atom trap near a nanoscale solid-state structure arises from the interference of an optical tweezer with its reflection from the cavity, which forms a standing-wave optical lattice. A photonic crystal waveguide cavity (PWC) is shown as an example structure. (b) Schematic of experimental apparatus. The trap is loaded with a single atom by displacing an optical tweezer from a nearby point in a free-space MOT. The trap is focused and steered by an aspheric lens (AL) and galvanometer mirror (M1). The presence of a single atom in the tweezer is detected by fluorescence on an avalanche photodiode (APD1), separated from the trap by a dichroic mirror (DM). (c) The coupling strength at a given distance from the outer surface of a PWC cavity with mode volume $V = 0.42\lambda^3$ (*24*). With a trap laser wavelength of 815 nm, the closest lattice site can be tuned from nearly 0-407 nm (shaded red), and the second lattice site from 407-815 nm (shaded blue). As discussed in the text, surface forces and currently realized trap depths limit the achievable distance to $z_0 \approx 100$ nm, at which point $2g/2\pi$ is several GHz.
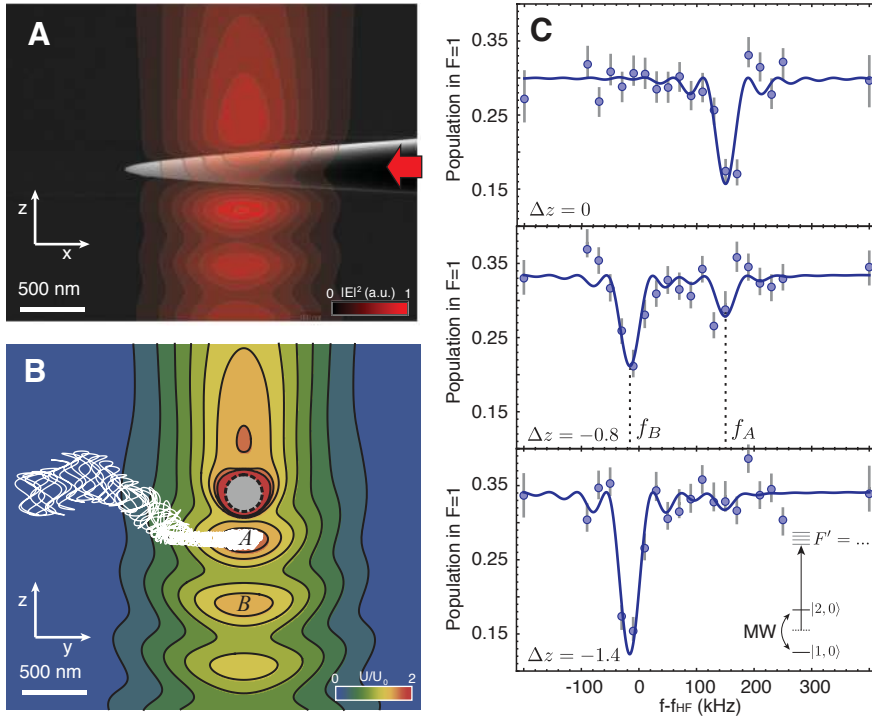
Figure 2: Loading the optical lattice near the surface. (a) A scanning electron microscope (SEM) image of a tapered nanofiber tip, overlaid with an FDTD simulation (red) of the optical tweezer intensity in the xz-plane. (b) Trapping potential, including surface forces (*24*), in the yz-plane; the grey circle is the fiber cross-section. The white solid line shows a typical simulated atomic trajectory for an atom with $E = 3k_B \times 10\mu K$. In the color scale, the potential is normalized to the maximum depth of the tweezer beam in free space, U_0. (c) Hyperfine transition spectra on the $|1,0\rangle \leftrightarrow |2,0\rangle$ transition, probing the atom-fiber separation. The (f_A, f_B) peaks show atoms loaded into the (first, second and higher) lattice sites. The focal plane of the tweezer is displaced by Δz from the fiber mid-plane in each panel; in this way, different lattice sites can be loaded. At at $\Delta z = 0$ we extract that $100^{+0}_{-12}\%$ of the atoms in the lattice are in the closest site (see text).
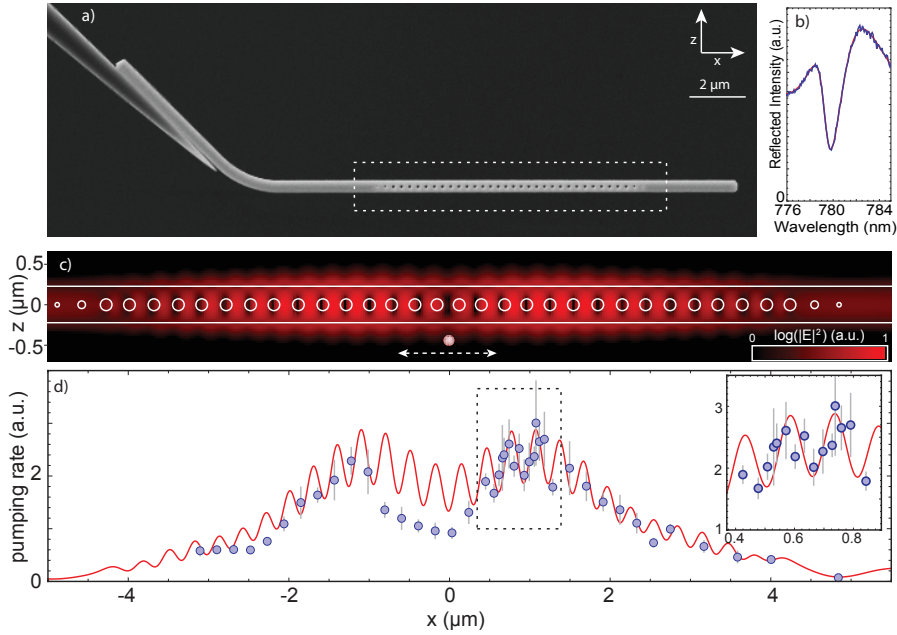
12

Figure 3: Coupling a single atom to a photonic crystal cavity. (a) An SEM image of a typical PWC attached to a tapered optical fiber. The fiber serves as both a mechanical support and an optical interface to the cavity. (b) Reflection spectrum of the PWC resonance near 780 nm, measured through the optical fiber. The line is a fit to a lorentzian plus a background of Fabry Perot modes of the waveguide, yielding $Q = 460(40)$ and $\lambda_0 = 779.5(1)$ (full spectrum in Fig. S5). (c) FDTD simulation of the PWC resonance at 779.5 nm, overlaid with a cross-section of the structure. The simulated mode volume is $V = 0.89\lambda^3$ (d) Measurement of the intensity distribution of the cavity using a trapped atom. Atoms are loaded at various positions indicated by the dashed arrow in panel (c), and the optical pumping rate from $F = 2 \rightarrow F = 1$ induced by the cavity field is measured. Error bars reflect one standard deviation in the fitted pumping rates. The red line shows a model based on FDTD simulations of the cavity mode convoluted with a Gaussian of 95 nm rms width, to incorporate for various broadening effects (see text). *Inset* In a set of points acquired in a continuous 32 hour window to minimize alignment drift, the standing wave structure of the cavity mode can be clearly resolved.
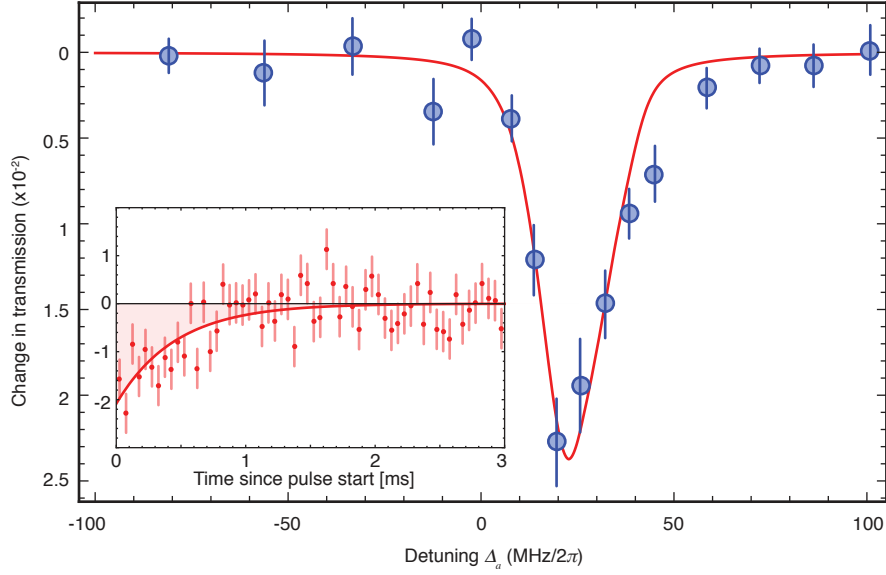
13

Figure 4: Change in cavity transmission from a single atom. Transmission of a weak probe beam tuned tuned to $F = 2 \rightarrow F = 3$ transition is measured vs. detuning from the atomic resonance $\Delta_a = \omega_l - \omega_a$, with $(\omega_l, \omega_a) =$ (laser, zero-field atomic transition) frequency. The cavity resonance remains fixed at $\omega_a + 0.3\kappa$. Error bars reflect one standard deviation in the fitted transmission reduction. The line is a fit to a numerical model described in the text, yielding $g = 580(80)$ MHz. *Inset* Transmission vs. time for cw probe pulse at $\Delta_a = 20$ MHz. The cavity transmission is initially suppressed; after several hundred microseconds the atom is heated by the probe laser and lost from the trap, restoring transmission. Error bars show shot noise in the number of detected photons. The shaded area represents the absence of 60 photons from the transmitted field.